The phase structure of a chirally invariant Higgs-Yukawa model

Lattice School 2007

Seattle, 27-Aug. 07

Philipp Gerhold[a]

Karl Jansen[b]

[a]Humboldt-Universität zu Berlin

[b]NIC, DESY (Zeuthen)

Deutsche Telekom Stiftung

Organization of the talk

- 1. Introduction and motivation
- 2. Phase structure at weak Yukawa coupling

  $\rightarrow$ Analytical large N_f-limit **vs.** Numerical results
- 3. Phase structure at strong Yukawa coupling

  $\rightarrow$ Analytical large N_f-limit **vs.** Numerical results
- 4. Outlook

Organization of the talk

- 1. Introduction and motivation
- 2. Phase structure at weak Yukawa coupling

  $\rightarrow$ Analytical large N_f-limit **vs.** Numerical results
- 3. Phase structure at strong Yukawa coupling

  $\rightarrow$ Analytical large N_f-limit **vs.** Numerical results
- 4. Outlook

Results published in	See also Talks at Lattice Conference by
arXiv: 0705:2539	Julius Kuti
arXiv: 0707:3849	Kieran Holland
	Daniel Nogradi

1.1 Introduction and motivation

- LHC will explore Higgs sector soon.
  $\rightarrow$ Theoretical predictions on Higgs properties are of particular interest now.
- Available theo. Higgs mass bounds depend strongly on perturbation theory.
  $\rightarrow$ Concerns that at least lower bound, based on vacuum instability, is fake (Kuti, Holland)
- Non-perturbative determination of Higgs mass bounds desired.
  $\rightarrow$ Study pure Top-Higgs sector with Higgs-Yukawa models.
- Earlier Higgs-Yukawa models explicitly broke chiral symmetry.
  - In continuum limit chiral symmetry restauration and lifting of fermion doublers could not be achieved simultaneously.

Study Higgs-Yukawa model with built-in chiral symmetry.

1.2 The model

- A chirally invariant Higgs-Yukawa model can be constructed using the Neuberger overlap operator $\mathcal{D}^{(N)}$ (Lüscher).
- The model, we consider, is discretized on a four-dimensional lattice with L sites per dimension (volume $V = L^4$).
- It contains one four-component, real Higgs field Φ, and N_f fermion doublets $\psi^{(i)}$, but **no gauge fields**:

$$Z = \int D\Phi \prod_{i=1}^{N_f} \left[D\psi^{(i)}\, D\bar{\psi}^{(i)} \right] \exp\left(-S_F^{kin} - S_Y - S_\Phi \right)$$

with kinetic fermion action S_F^{kin}, Yukawa coupling term S_Y, and Higgs action S_Φ.

1.2 The model

- A chirally invariant Higgs-Yukawa model can be constructed using the Neuberger overlap operator $\mathcal{D}^{(N)}$ (Lüscher).
- The model, we consider, is discretized on a four-dimensional lattice with L sites per dimension (volume $V = L^4$).
- It contains one four-component, real Higgs field Φ, and N_f fermion doublets $\psi^{(i)}$, but **no gauge fields**:

$$Z = \int D\Phi \prod_{i=1}^{N_f} \left[D\psi^{(i)}\, D\bar{\psi}^{(i)} \right] \exp\left(-S_F^{kin} - S_Y - S_\Phi \right)$$

with kinetic fermion action S_F^{kin}, Yukawa coupling term S_Y, and Higgs action S_Φ.

- Kinetic fermion action:

$$S_F^{kin} = \sum_{i=1}^{N_f} \bar{\psi}^{(i)} \mathcal{D}^{(N)} \psi^{(i)}$$

1.3 The model

- The Yukawa coupling term is given as

$$S_Y = y_N \sum_{i=1}^{N_f} \bar{\psi}^{(i)} B \cdot \left[\mathbb{1} - \frac{1}{2\rho} \mathcal{D}^{(N)} \right] \psi^{(i)}$$

$$B_{x,y} = \mathbb{1}_{x,y} \frac{(1-\gamma_5)}{2} \phi_x + \mathbb{1}_{x,y} \frac{(1+\gamma_5)}{2} \phi_x^\dagger$$

where the Higgs field Φ_x is written as quaternion ϕ_x acting on flavor index

$$\phi_x = \Phi_x^0 \mathbb{1} - i(\Phi_x^1 \tau_1 + \Phi_x^2 \tau_2 + \Phi_x^3 \tau_3), \quad \tau_i : \text{Pauli-matrices.}$$

1.3 The model

- The Yukawa coupling term is given as

$$S_Y = y_N \sum_{i=1}^{N_f} \bar{\psi}^{(i)} B \cdot \left[\mathbb{1} - \frac{1}{2\rho} \mathcal{D}^{(N)} \right] \psi^{(i)}$$

$$B_{x,y} = \mathbb{1}_{x,y} \frac{(1-\gamma_5)}{2} \phi_x + \mathbb{1}_{x,y} \frac{(1+\gamma_5)}{2} \phi_x^\dagger$$

where the Higgs field Φ_x is written as quaternion ϕ_x acting on flavor index

$$\phi_x = \Phi_x^0 \mathbb{1} - i(\Phi_x^1 \tau_1 + \Phi_x^2 \tau_2 + \Phi_x^3 \tau_3), \quad \tau_i : \text{Pauli-matrices.}$$

- The Higgs action S_Φ in lattice notation is

$$S_\Phi = -\kappa_N \sum_{x,\mu} \Phi_x^\dagger \left[\Phi_{x+\hat{\mu}} + \Phi_{x-\hat{\mu}} \right] + \sum_x \Phi_x^\dagger \Phi_x + \lambda_N \sum_x \left(\Phi_x^\dagger \Phi_x - N_f \right)^2$$

related to usual notation by transforming couplings $(\kappa_N, \lambda_N) \leftrightarrow (\kappa, \lambda)$.

2.1 Phase structure at small y_N

- We consider the limit $N_f \to \infty$ where the couplings scale according to

$$y_N = \frac{\tilde{y}_N}{\sqrt{N_f}},\ \tilde{y}_N = \text{const} \qquad \lambda_N = \frac{\tilde{\lambda}_N}{N_f},\ \tilde{\lambda}_N = \text{const} \qquad \kappa_N = \tilde{\kappa}_N,\ \tilde{\kappa}_N = \text{const}$$

- The effective action

$$S_{eff}[\Phi] \quad = \quad S_\Phi[\Phi] - N_f \cdot \log\left[\det\left(y_N B\mathcal{D}^{(N)} - 2\rho\mathcal{D}^{(N)} - 2\rho B\right)\right]$$

  can be evaluated at least for the constant and staggered modes of Φ.

- For the Higgs field we take a magnetization (m) and a staggered magnetization (s) into account by the ansatz

$$\Phi(x) = \hat{\Phi} \cdot \sqrt{N_f} \cdot \left(m + s \cdot (-1)^{\sum_{\mu=0}^{3} x_\mu} \right)$$

  where $\hat{\Phi} \in \mathbb{R}^4$, $|\hat{\Phi}| = 1$ is a constant unit vector and $m, s \in \mathbb{R}$.

2.2 Effective Potential

- At tree-level one finally finds for the effective potential $V(m,s)$

$$\begin{aligned}
\frac{V(m,s)}{L^4 N_f} &= m^2 + s^2 - 8\tilde{\kappa}_N\left(m^2 - s^2\right) + \tilde{\lambda}_N\left(m^4 + s^4 + 6m^2s^2 - 2\left(m^2 + s^2\right)\right) \\
&- \frac{1}{L^4}\sum_{p\in\mathcal{P}} \log\Bigg[\left(\left|\nu^+(p)\right|\left|\nu^+(\wp)\right| + \frac{\tilde{y}_N^2}{4\rho^2}\left(m^2 - s^2\right)\left|\nu^+(p) - 2\rho\right|\left|\nu^+(\wp) - 2\rho\right|\right)^2 \\
&+ m^2\frac{\tilde{y}_N^2}{4\rho^2}\left(\left|\nu^+(p) - 2\rho\right|\cdot\left|\nu^+(\wp)\right| - \left|\nu^+(\wp) - 2\rho\right|\cdot\left|\nu^+(p)\right|\right)^2\Bigg]^2
\end{aligned}$$

with

$$\begin{aligned}
p &= (p_0, p_1, p_2, p_3) \in \mathcal{P} : \text{allowed lattice momenta} \\
\nu(p) &: \text{eigenvalues of Neuberger Dirac operator } \hat{\mathcal{D}}^{(N)} \\
\wp_\mu &= p_\mu + \pi
\end{aligned}$$

- The phase diagram can be explored by numerically searching for the absolute minima of the effective action with respect to m and s.

2.3 Analytical phase diagrams

In general, four different phases can be obtained in this ansatz:

- SYM: $m = 0$, $s = 0$
- FM: $m \neq 0$, $s = 0$
- AFM: $m = 0$, $s \neq 0$
- FI: $m \neq 0$, $s \neq 0$

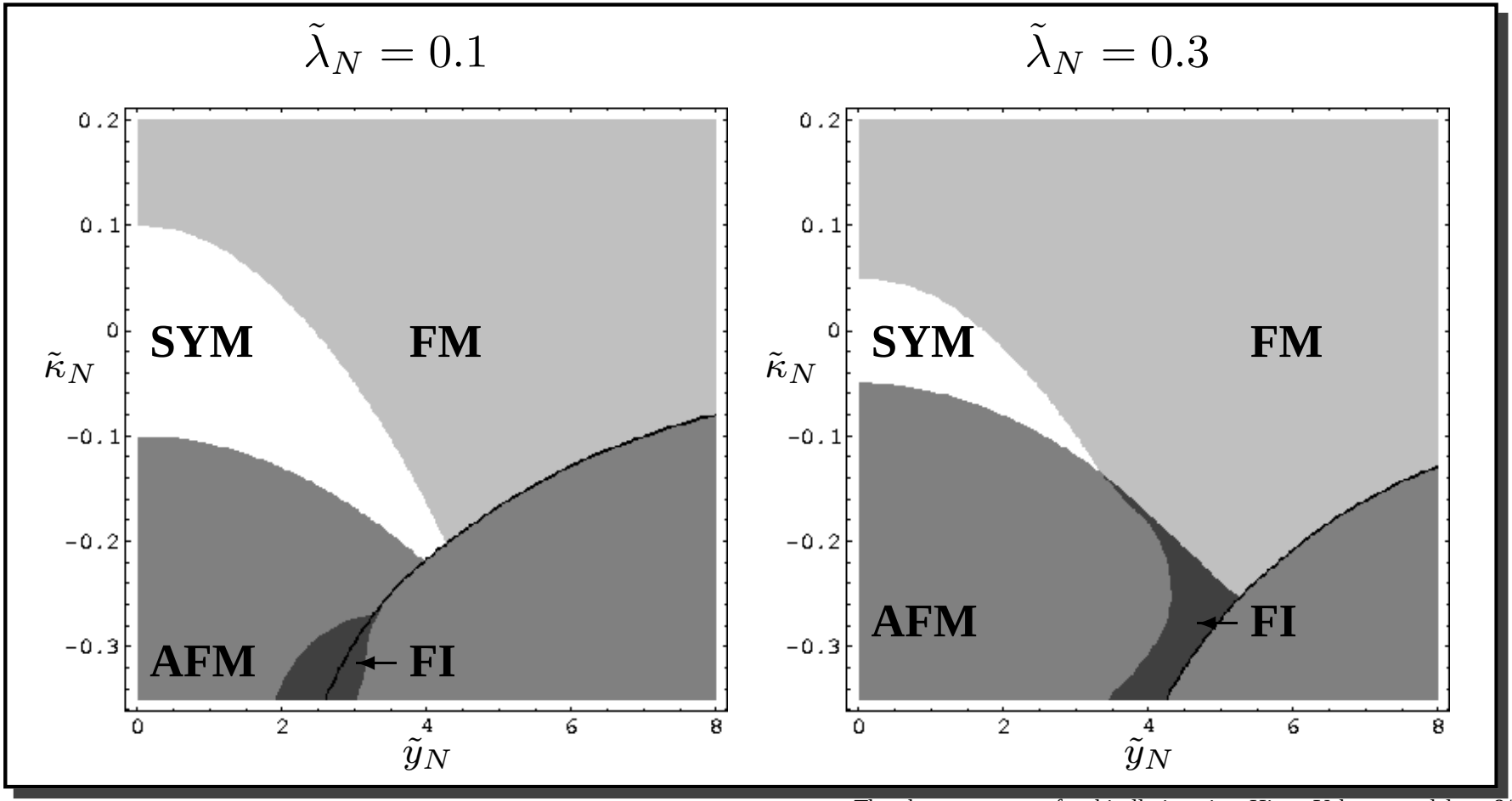

2.4 MC-simulations: Definitions

- We have implemented an HMC-algorithm for even values of N_f

2.4 MC-simulations: Definitions

- We have implemented an HMC-algorithm for even values of N_f
- As observables we consider the (staggered) magnetization m (s)

$$m = \left[\sum_{i=0}^{3} \left| \frac{1}{L^4} \sum_n \Phi_n^i \right|^2 \right]^{\frac{1}{2}}, \qquad s = \left[\sum_{i=0}^{3} \left| \frac{1}{L^4} \sum_n (-1)^{\sum_\mu n_\mu} \cdot \Phi_n^i \right|^2 \right]^{\frac{1}{2}}$$

and the corresponding (staggered) susceptibility χ_m (χ_s)

$$\chi_m = L^4 \cdot \left[\langle m^2 \rangle - \langle m \rangle^2 \right], \qquad \chi_s = L^4 \cdot \left[\langle s^2 \rangle - \langle s \rangle^2 \right],$$

where $\langle ... \rangle$ denotes the average over the generated Φ-field configurations.

2.4 MC-simulations: Definitions

- We have implemented an HMC-algorithm for even values of N_f
- As observables we consider the (staggered) magnetization m (s)

$$m = \left[\sum_{i=0}^{3} \left| \frac{1}{L^4} \sum_n \Phi_n^i \right|^2 \right]^{\frac{1}{2}}, \qquad s = \left[\sum_{i=0}^{3} \left| \frac{1}{L^4} \sum_n (-1)^{\sum_\mu n_\mu} \cdot \Phi_n^i \right|^2 \right]^{\frac{1}{2}}$$

and the corresponding (staggered) susceptibility χ_m (χ_s)

$$\chi_m = L^4 \cdot \left[\langle m^2 \rangle - \langle m \rangle^2 \right], \qquad \chi_s = L^4 \cdot \left[\langle s^2 \rangle - \langle s \rangle^2 \right],$$

where $\langle ... \rangle$ denotes the average over the generated Φ-field configurations.

- Determine phase transition point by fit of $\chi_{m,s}$ to finite-size-scaling ansatz

$$\chi_{m,s} = A_1^{m,s} \cdot \left(\frac{1}{L^{-2/\nu} + A_{2,3}^{m,s} (\kappa_N - \kappa_{\text{crit}}^{m,s})^2} \right)^{\gamma/2},$$

with fitting parameters $\kappa_{\text{crit}}^{m,s}, A_1^{m,s}, A_2^{m,s}, A_3^{m,s}$.

2.5 Phase structure overview

- Numerically we find the expected phases at the predicted locations.
- Qualitatively, the phase diagram is in very good agreement with the large N_f analysis.

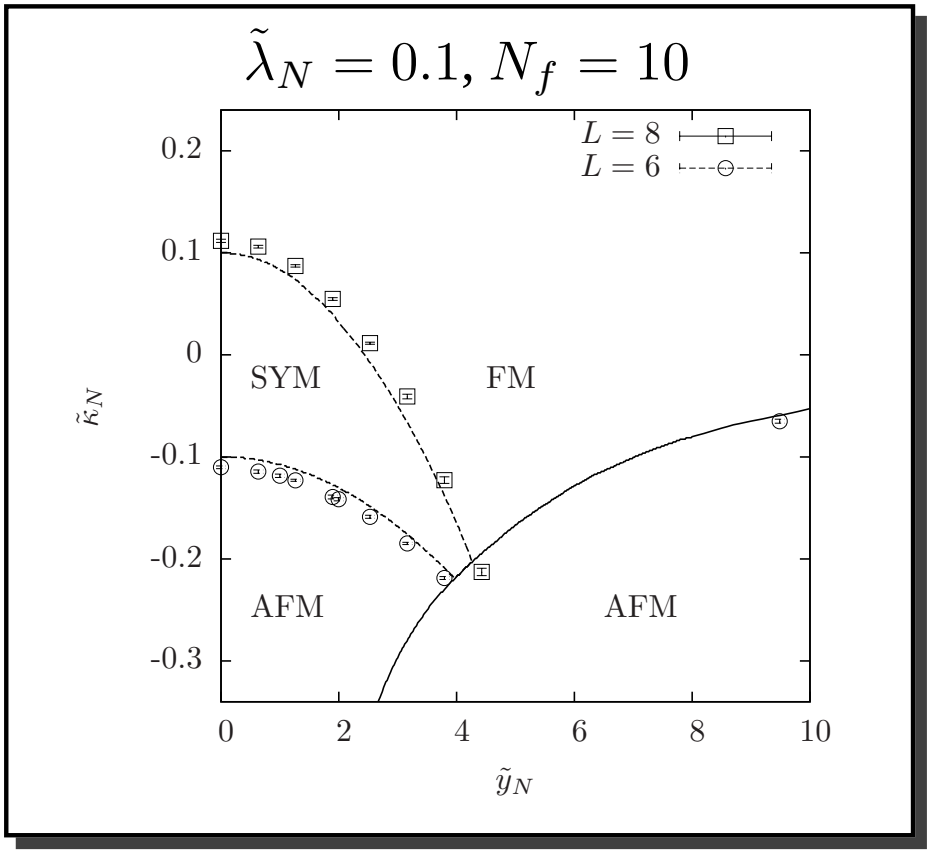

2.6 Finite Size Effects

- Phase transition lines strongly shifted by finite size effects.
- We isolate finite size effects from $1/N_f$-corrections by choice $N_f = 50$.
- We compare $L = 4$ and $L = 8$ results with analytical finite size expectations

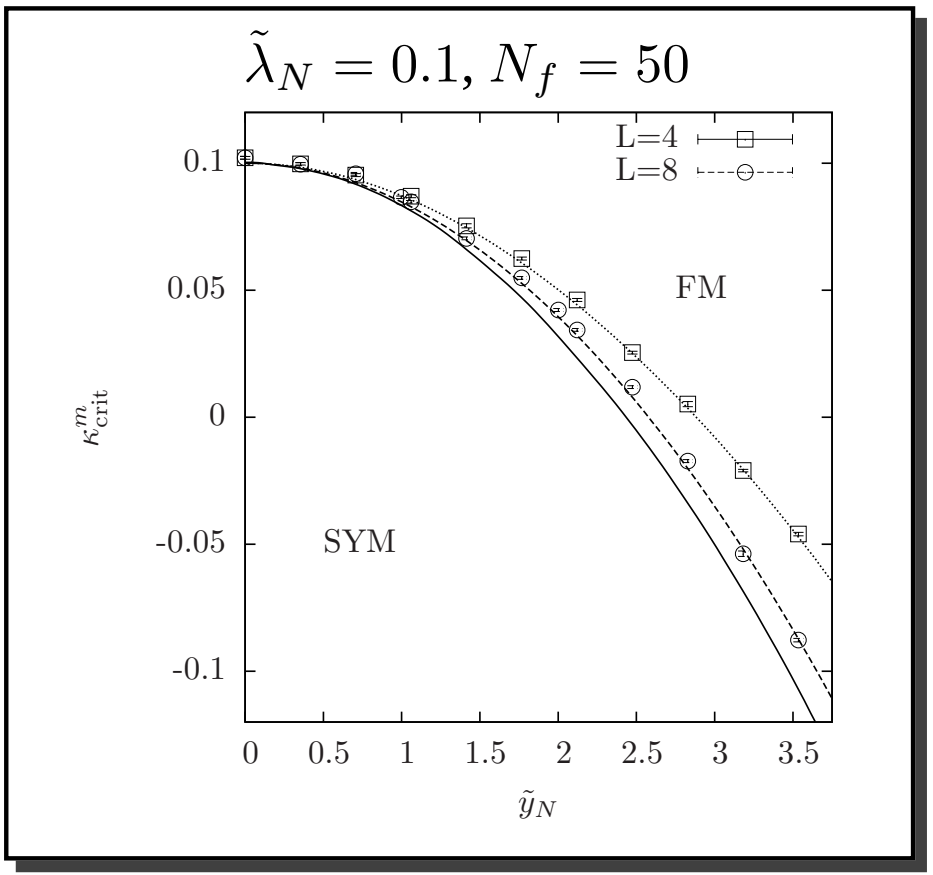

2.7 $1/N_f$ corrections

- We demonstrate strength of $1/N_f$-corrections by determining phase transition points $\kappa_{\rm crit}^{m,s}$ for several values of N_f.
- To isolate $1/N_f$-corrections from finite size effects we compare with analytical, finite size expectations.

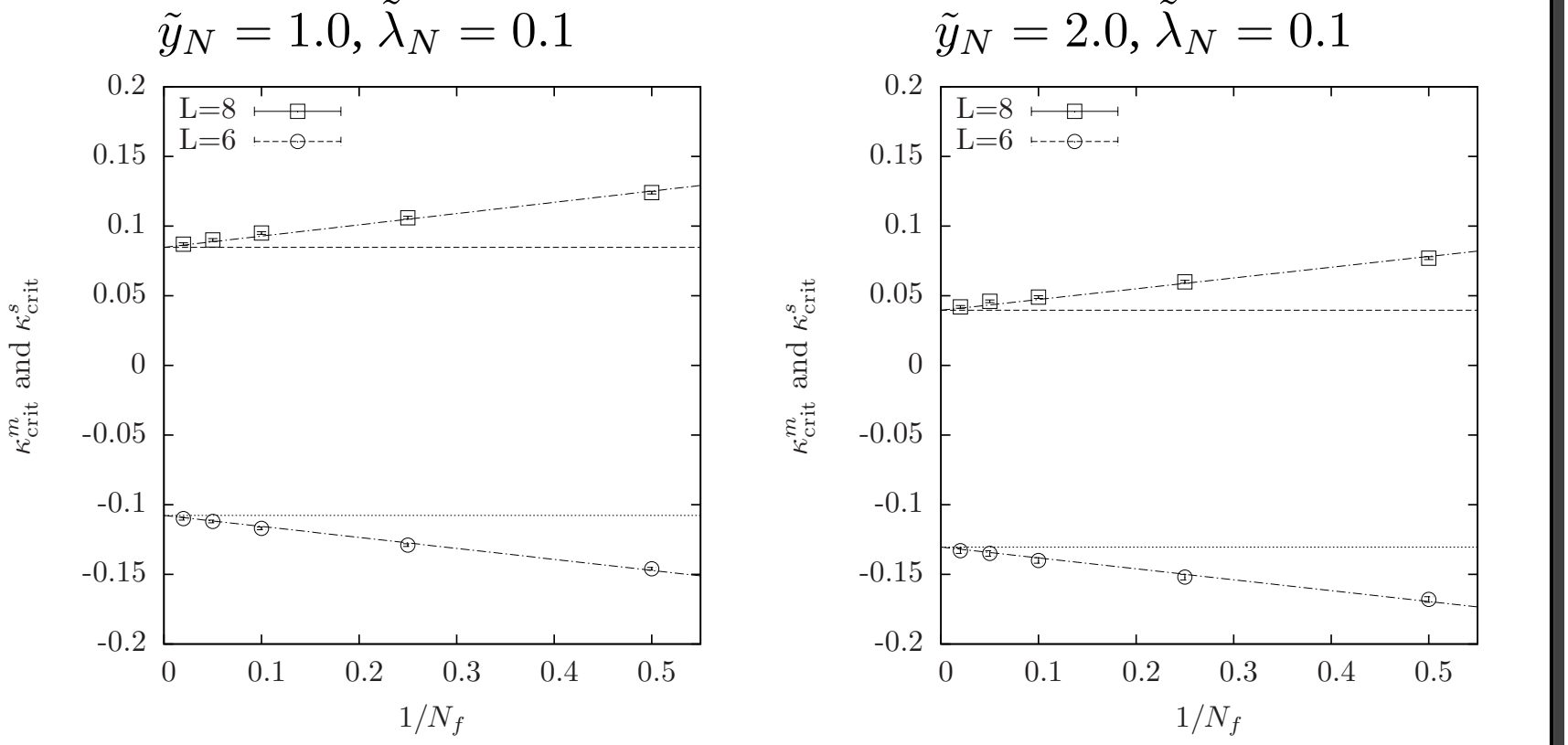

3.1 Phase structure at large y_N

- Idea: Divide out $y_N B(\mathcal{D}^{(N)} - 2\rho)$ and develop logarithm into power series

$$S_{eff}[\Phi] \quad = \quad S_\Phi - N_f \cdot \log\left[\det\left(y_N B\mathcal{D}^{(N)} - 2\rho\mathcal{D}^{(N)} - 2\rho B\right)\right]$$

3.1 Phase structure at large y_N

- Idea: Divide out $y_N B(\mathcal{D}^{(N)} - 2\rho)$ and develop logarithm into power series

$$
\begin{aligned}
S_{eff}[\Phi] &= S_\Phi - N_f \cdot \log\left[\det\left(y_N B\mathcal{D}^{(N)} - 2\rho\mathcal{D}^{(N)} - 2\rho B\right)\right] \\
&\to S_\Phi - N_f \cdot \log\left[\det\left(\mathbb{1} - \frac{2\rho}{y_N}\mathcal{D}^{(N)}\left[\mathcal{D}^{(N)} - 2\rho\right]^{-1} B^{-1}\right)\right] \\
&\to S_\Phi - N_f \sum_x log(|\Phi_x|^8) - N_f \frac{(4\rho)^2}{y_N^2} \sum_{x,y} \frac{\Phi_x^\dagger K_{x,y} \Phi_y}{|\Phi_x|^2 \cdot |\Phi_y|^2}
\end{aligned}
$$

where the coupling matrix $K_{x,y}$ is explicitly known.

3.1 Phase structure at large y_N

- Idea: Divide out $y_N B(\mathcal{D}^{(N)} - 2\rho)$ and develop logarithm into power series

$$
\begin{aligned}
S_{eff}[\Phi] &= S_\Phi - N_f \cdot \log\left[\det\left(y_N B\mathcal{D}^{(N)} - 2\rho\mathcal{D}^{(N)} - 2\rho B\right)\right] \\
&\to S_\Phi - N_f \cdot \log\left[\det\left(\mathbb{1} - \frac{2\rho}{y_N}\mathcal{D}^{(N)}\left[\mathcal{D}^{(N)} - 2\rho\right]^{-1} B^{-1}\right)\right] \\
&\to S_\Phi - N_f \sum_x log(|\Phi_x|^8) - N_f \frac{(4\rho)^2}{y_N^2} \sum_{x,y} \frac{\Phi_x^\dagger K_{x,y} \Phi_y}{|\Phi_x|^2 \cdot |\Phi_y|^2}
\end{aligned}
$$

  where the coupling matrix $K_{x,y}$ is explicitly known.

- In large N_f-limit amplitude $|\Phi_x|$ becomes fixed.

> The model becomes an $O(4)$-symmetric sigma-model leading to the existence of a symmetric phase at strong Yukawa couplings.

3.1 Phase structure at large y_N

- Idea: Divide out $y_N B(\mathcal{D}^{(N)} - 2\rho)$ and develop logarithm into power series

$$\begin{aligned} S_{eff}[\Phi] &= S_\Phi - N_f \cdot \log\left[\det\left(y_N B\mathcal{D}^{(N)} - 2\rho\mathcal{D}^{(N)} - 2\rho B\right)\right] \\ &\to S_\Phi - N_f \cdot \log\left[\det\left(\mathbb{1} - \frac{2\rho}{y_N}\mathcal{D}^{(N)}\left[\mathcal{D}^{(N)} - 2\rho\right]^{-1} B^{-1}\right)\right] \\ &\to S_\Phi - N_f \sum_x log(|\Phi_x|^8) - N_f \frac{(4\rho)^2}{y_N^2} \sum_{x,y} \frac{\Phi_x^\dagger K_{x,y} \Phi_y}{|\Phi_x|^2 \cdot |\Phi_y|^2} \end{aligned}$$

  where the coupling matrix $K_{x,y}$ is explicitly known.

- Caution: $\mathcal{D}^{(N)} - 2\rho$ has zero modes: More careful calculation yields

$$\begin{aligned} S_{eff}[\Phi] &\to S_\Phi - N_f \sum_x log(|\Phi_x|^8) - N_f \frac{(4\rho)^2}{y_N^2} \sum_{x,y} \frac{\Phi_x^\dagger K_{x,y} \Phi_y}{|\Phi_x|^2 \cdot |\Phi_y|^2} \\ &- N_f \cdot \log\det{}^*\left(B^{-1}\right) - N_f \cdot \log\det{}^*\left(\mathbb{1} + \frac{2\rho}{y_N} F[\Phi]\right) \end{aligned}$$

  where $\det^*$ is the determinant over zero-modes (120 modes) and $F[\Phi]$ can be explicitly given.

3.2 Analytical Phase Diagrams

- Neglecting the finite-volume terms, the phase structure can be derived in the large N_f-limit applying the ansatz

$$y_N = \tilde{y}_N,\ \tilde{y}_N = \text{const}, \quad \lambda_N = \frac{\tilde{\lambda}_N}{N_f},\ \tilde{\lambda}_N = \text{const}, \quad \kappa_N = \frac{\tilde{\kappa}_N}{N_f},\ \tilde{\kappa}_N = \text{const},$$

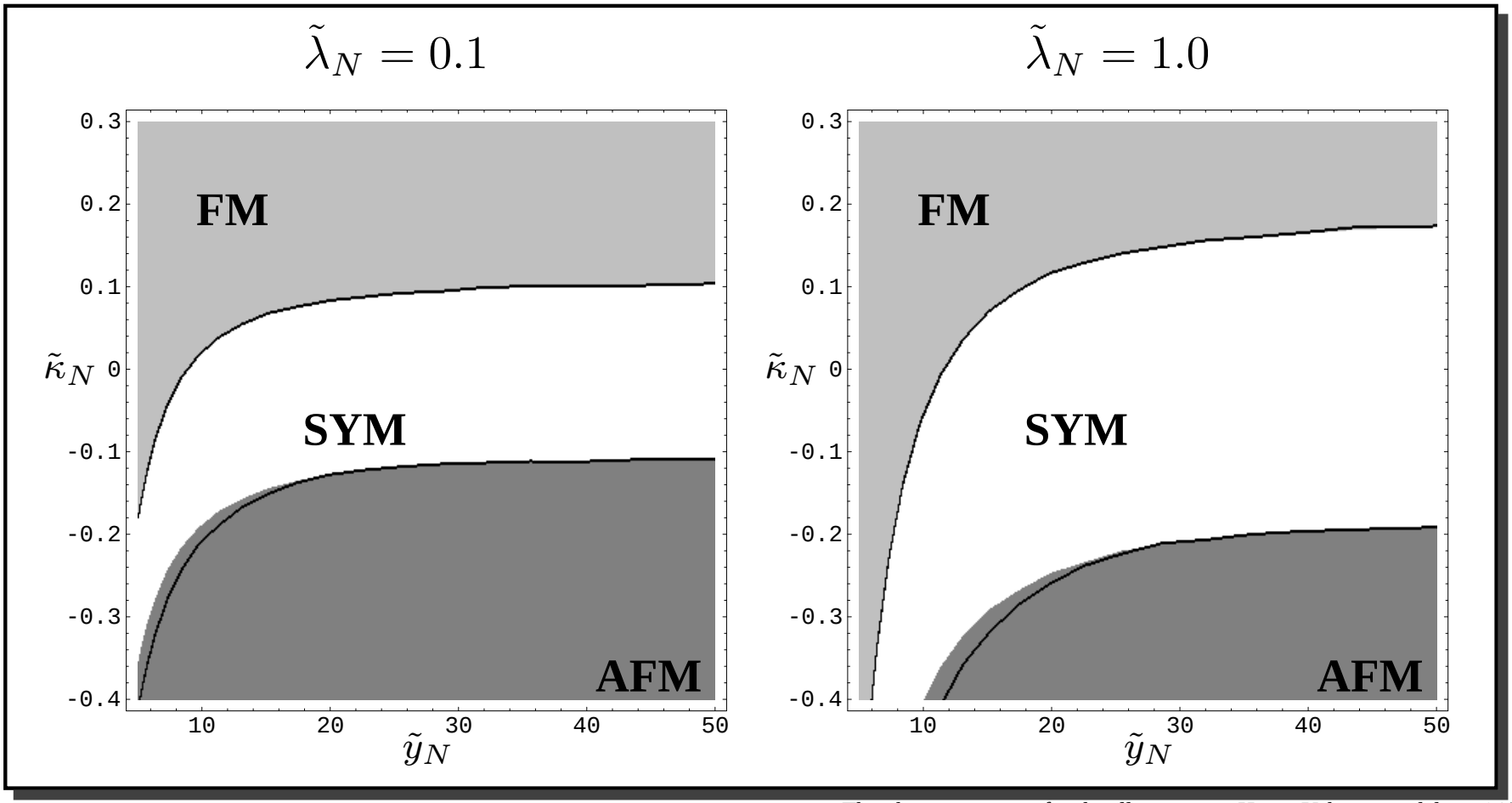

3.3 MC-results: Magnetizations

- We show the (staggered) magnetization for varying κ_N at $\tilde{\lambda}_N = 0.1$, $\tilde{y}_N = 30$ for different lattice sizes.
- Strong finite volume effects prevent emergence of the symmetric phase on too small lattices and cause asymmetry in m and s.

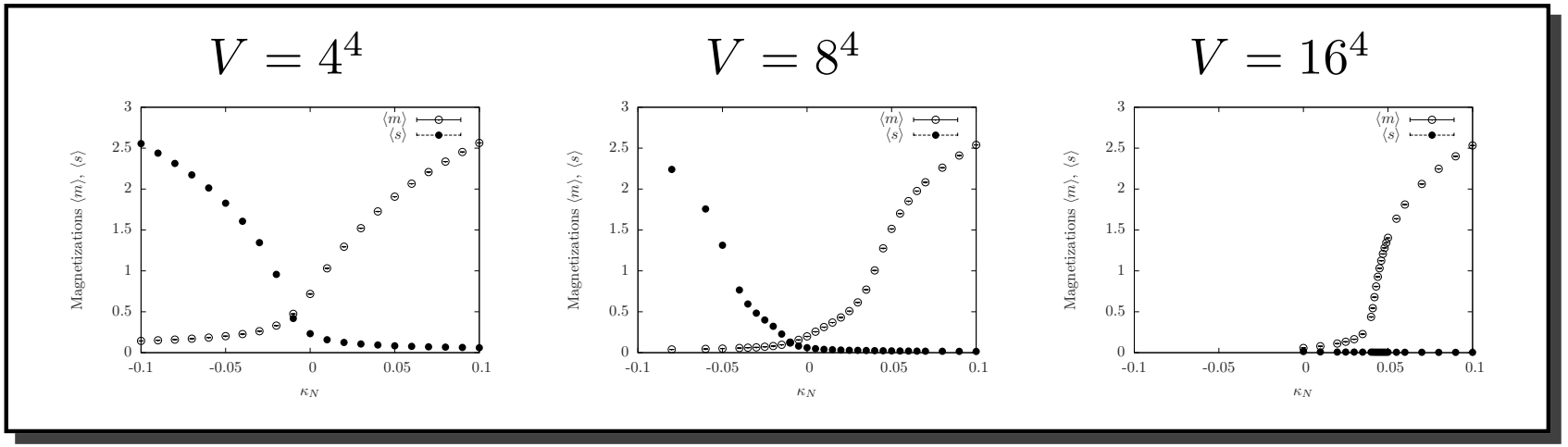

3.3 MC-results: Magnetizations

- We show the (staggered) magnetization for varying κ_N at $\tilde{\lambda}_N = 0.1$, $\tilde{y}_N = 30$ for different lattice sizes.
- Strong finite volume effects prevent emergence of the symmetric phase on too small lattices and cause asymmetry in m and s.

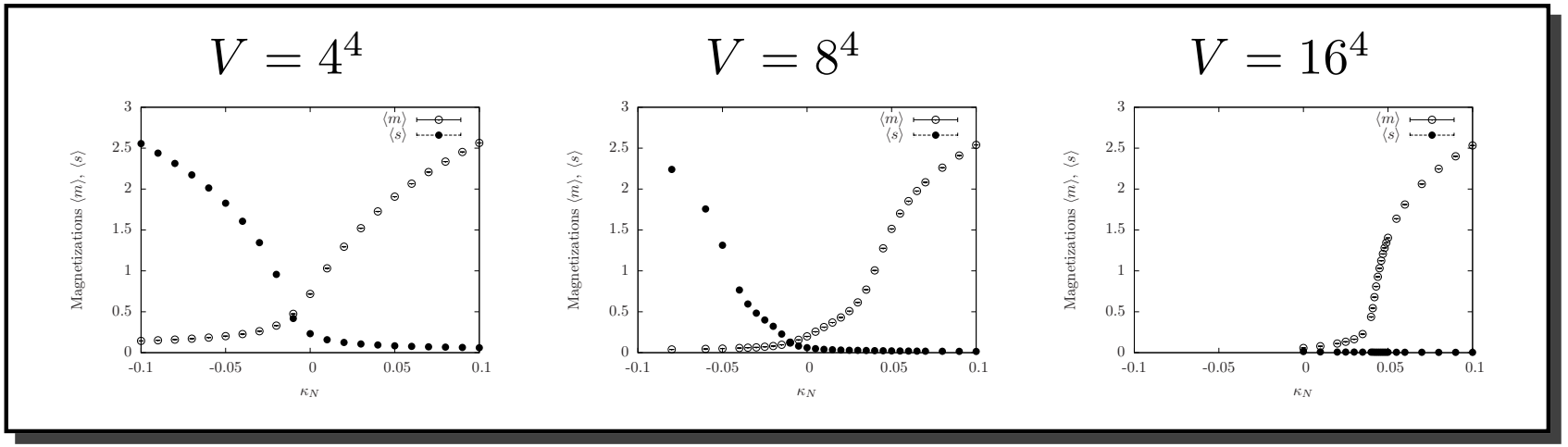

- Strongest finite-volume contribution is $\log \det{}^* \left(B^{-1}\right)$.
  It can be written in terms of m and s, explaining the observations

$$-N_f \log \det{}^* \left(B^{-1}\right) = \text{Const} - 8N_f \log|m| + 64N_f \log\left|m^2 - s^2\right|$$

3.4 MC-results: Susceptibilities

- We show the magnetic susceptibilities for varying κ_N at $\tilde{\lambda}_N = 0.1$, $\tilde{y}_N = 30$ for different lattice sizes.
- On small lattices ($V = 4^4$) the maximum is at $\kappa_N = 0$, caused by the finite-volume effects.
- On larger lattices ($V = 8^4$) a second peak develops at $\kappa_N = 0.04$, which describes the location of the physical phase transition

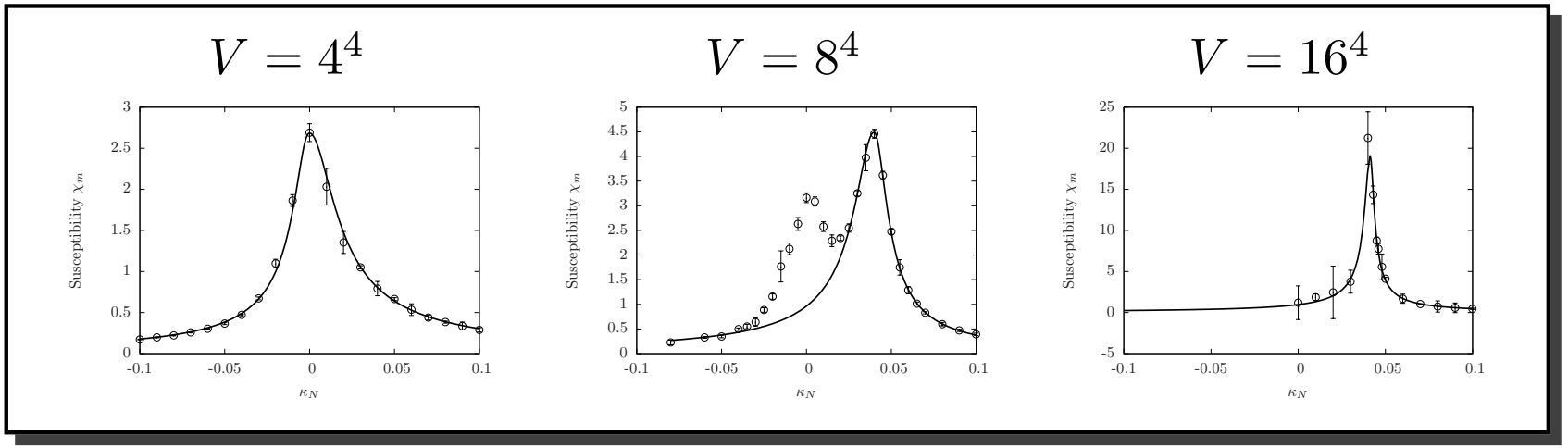

3.5 Phase Diagram

- We compare numerical and analytical results for the SYM-FM transition line.
- Good agreement is found even at $N_f = 2$.
- The SYM-AFM phase transition line was numerically too demanding for our HMC-algorithm.

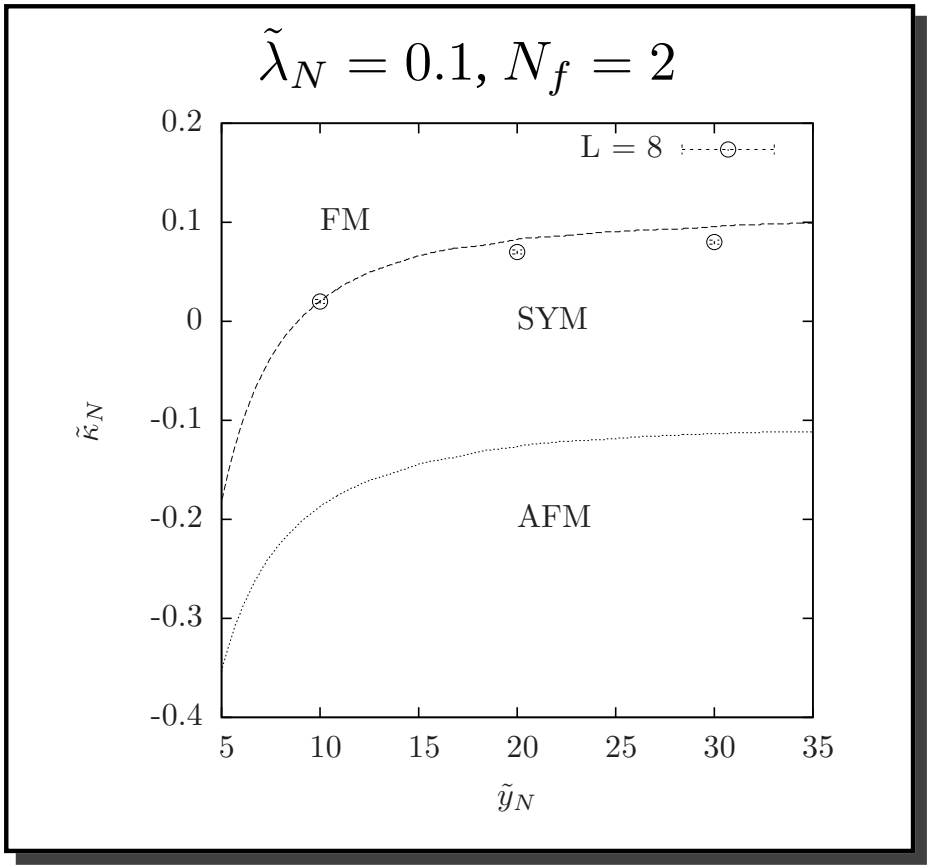

Summary and Outlook

- Large N_f analysis gives good understanding of qualitative phase structure.
- Finite size effects can be quantitatively described in large N_f-limit.
- A symmetric phase exists also at strong Yukawa coupling.
- First results on upper Higgs mass bound will become available soon.

2.8 Evidence for FI-phase

- Also numerical evidence for the predicted FI-phase with

$$\langle m \rangle > 0 \text{ and } \langle s \rangle > 0$$

  deeply inside the anti-ferromagnetic phase can be found.

- The plots were made for $\tilde{\lambda}_N = 0.1$, $N_f = 10$, $L = 6$.

Magnetizations

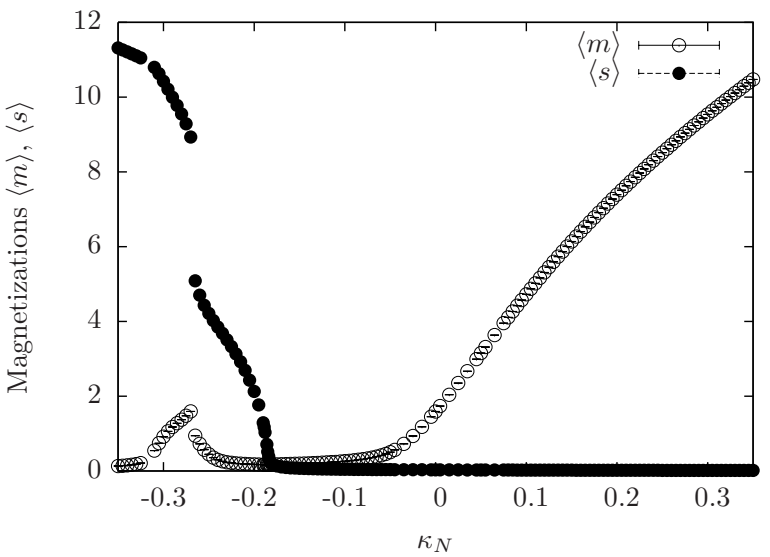

Susceptibility χ_m

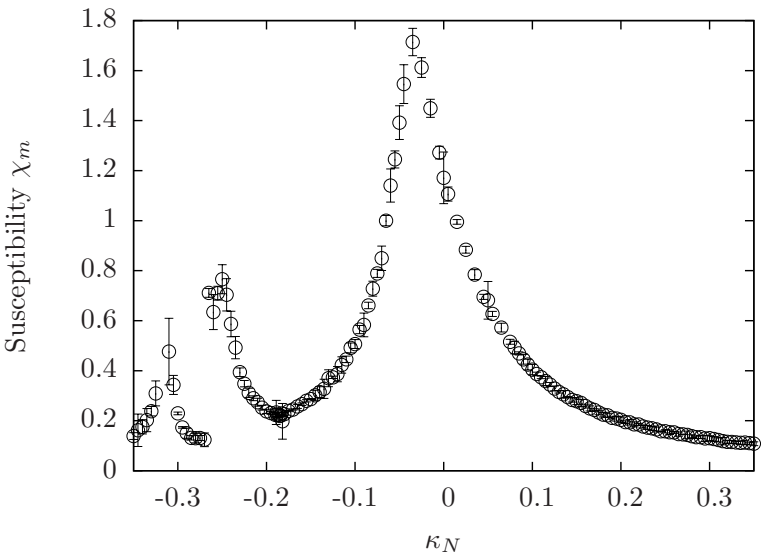

4.1 Towards Upper Mass Bounds:

- VERY PRELIMINARY
- To access physical setting $N_f = 1$, we implemented a PHMC-algorithm.
- We fixed physical scale by phenomenological value $vev = 246\,\text{GeV}$
- We searched for the physical region in the phase diagram by fixing the top quark mass to $m_{top} = 175\,\text{GeV}$.
- To obtain upper mass bound, we went to strong quartic couplings λ_N.
- As a first step, we simulated the model on a $16^3 \times 32$ lattice close to the phase transition in the FM-phase.
- To account for the 3 Goldstone-modes we split the 4-component Higgs field into its radial ϕ and tangential components $\vec{\pi}$.

4.2 Goldstone - Propagator:

- Obtain Goldstone renormalization factor Z_G from inverse propagator of massless Goldstone-modes

$$G_\pi^{-1}(\hat{p}^2) = \frac{\hat{p}^2}{Z_G}$$

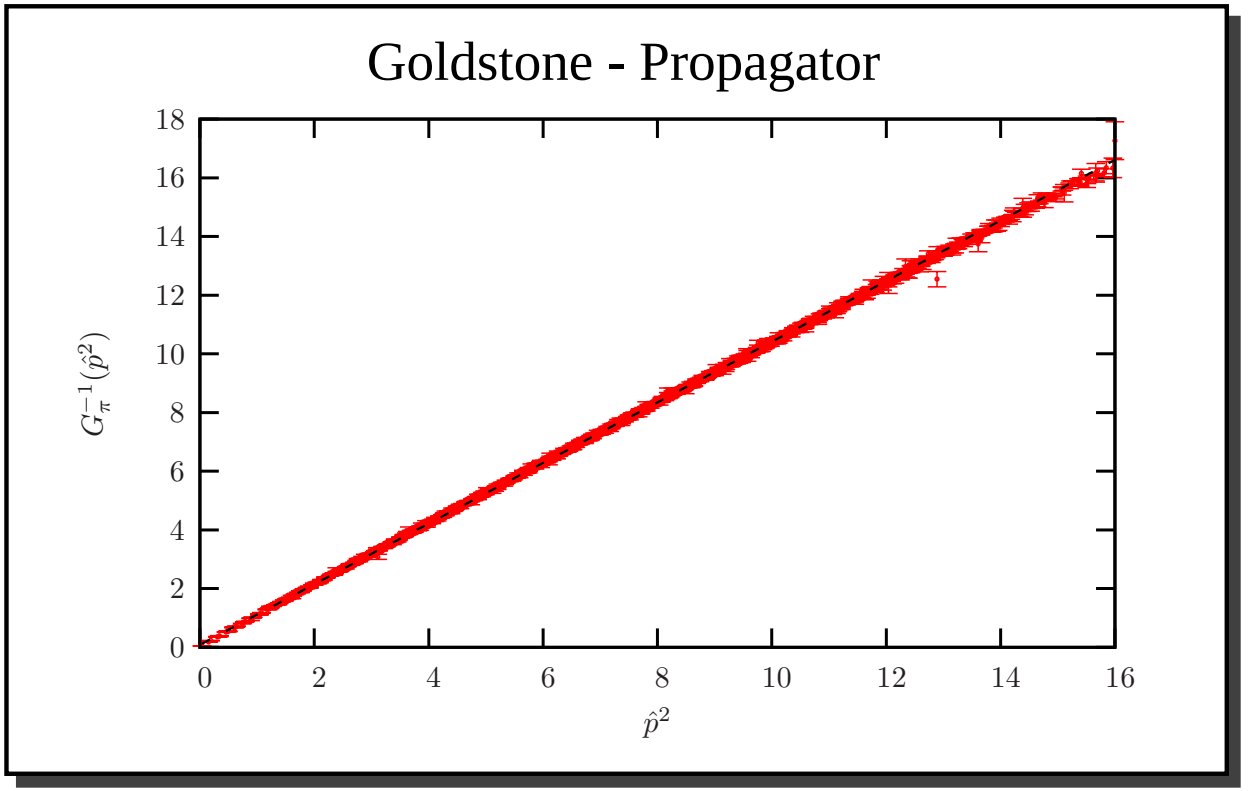

$$Z_G = 0.9683 \pm 0.0002$$

4.3 Higgs - Propagator:

- Obtain Higgs propagator-mass $m_{H,prop}$ from propagator of Higgs-mode

$$G_{\phi}^{-1}(\hat{p}^2) = \frac{\hat{p}^2 + m_{H,prop}^2}{Z_H}$$

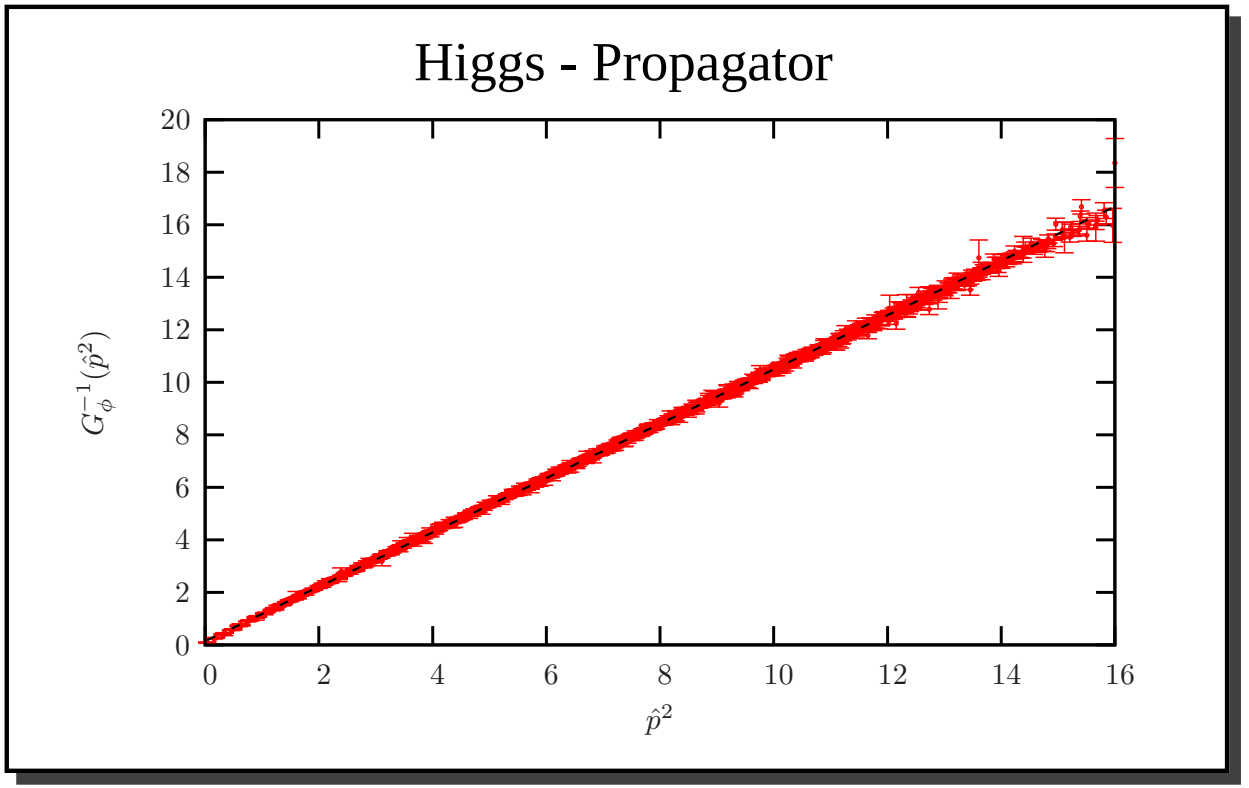

$$m_{H,prop} = 0.384 \pm 0.009$$

4.4 Fermion correlator:

- Obtain top quark mass m_{top} from fermion correlator $\langle \psi_{t_1} \bar{\psi}_{t_2} \rangle$

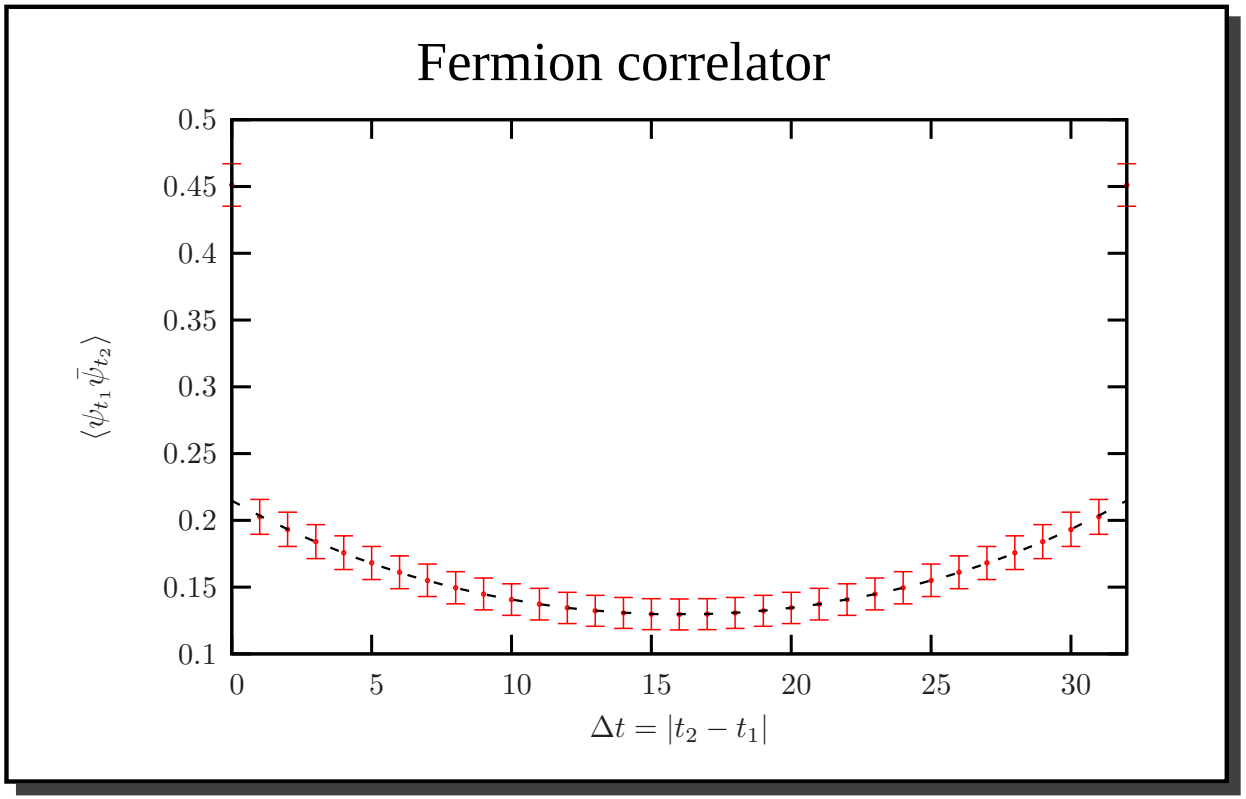

$$m_{top} = 0.0686 \pm 0.0021$$

4.5 Higgs correlator:

- Obtain Higgs mass m_H from Higgs correlator $\langle \phi_{t_1} \phi_{t_2} \rangle$

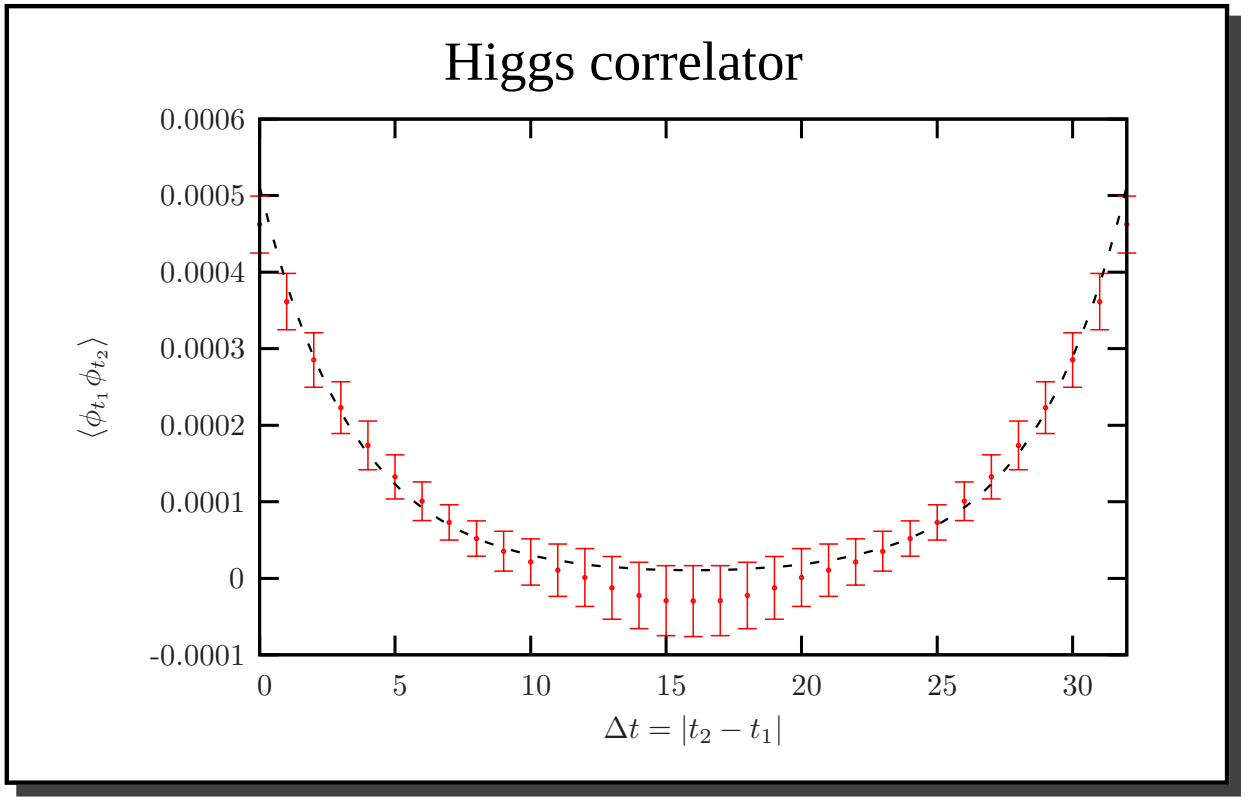

$$m_H = 0.286 \pm 0.011$$

4.5 Summary of results:

Cut-off Λ	(2591 ± 58) GeV
Top mass m_{top}	(178.8 ± 6.8) GeV
Higgs mass m_H	(741 ± 29) GeV
Higgs prop. mass $m_{H,prop}$	(994 ± 22) GeV
Bare Lambda λ_0	4.4
Ren. Lambda λ_{ren}	4.53 ± 0.18
Ren. y y_{ren}	0.723 ± 0.027

Finite Size Effects

Magnetizations

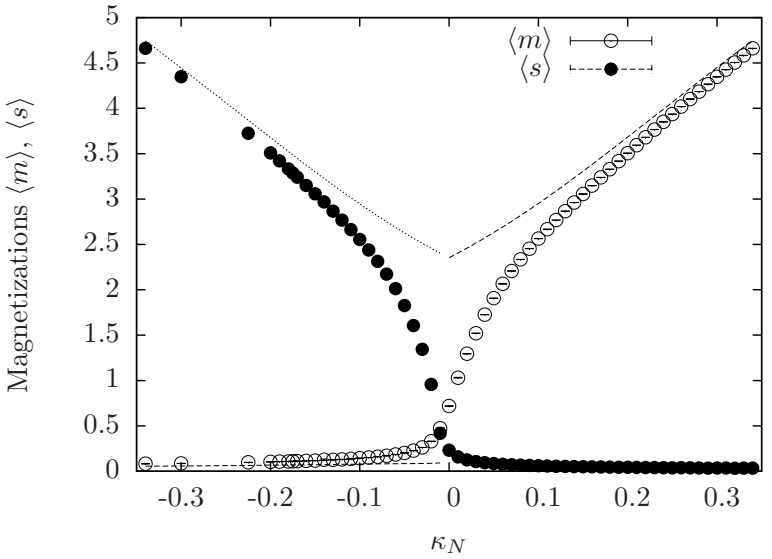

Susceptibility χ_m